HHS Public Access

Author manuscript

Nat Commun. Author manuscript; available in PMC 2015 September 25.

Published in final edited form as:

Nat Commun. ; 6: 6626. doi:10.1038/ncomms7626.

Generation and Expansion of highly-pure Motor Neuron Progenitors from Human Pluripotent Stem Cells

Zhong-Wei Du[1,*,#], **Hong Chen**[1,2,*], **Huisheng Liu**[1], **Jianfeng Lu**[1], **Kun Qian**[1,3], **Cindy Tzu-Ling. Huang**[1], **Xiaofen Zhong**[1], **Frank Fan**[4], and **Su-Chun Zhang**[1,5,#]

[1]Waisman Center, University of Wisconsin, Madison, WI 53705, USA

[2]Department of Rehabilitation Medicine, Tongji Hospital, Tongji Medical College, Huazhong University of Science and Technology, Wuhan, 430030, China

[3]Reproductive Medicine Center, Tongji Hospital, Tongji Medical College, Huazhong University of Science and Technology, Wuhan, 430030, China

[4]Promega Corporation, Madison, WI 53711, USA

[5]Department of Neuroscience and Department of Neurology, School of Medicine and Public Health, University of Wisconsin, Madison, WI 53705, USA

SUMMARY

Human pluripotent stem cells (hPSCs) have opened new opportunities for understanding human development, modeling disease processes and developing new therapeutics. However, these applications are hindered by low-efficiency and heterogeneity of target cell types differentiated from hPSCs, such as motor neurons (MNs), as well as our inability to maintain the potency of lineage committed progenitors. Here, by using a combination of small molecules that regulate multiple signaling pathways, we develop a method to guide human embryonic stem cells to a near-pure population (>95%) of motor neuron progenitors (MNPs) in 12 days, and an enriched population (>90%) of functionally mature MNs in an additional 16 days. More importantly, the MNPs can be expanded for at least 5 passages so that a single MNP can be amplified to 1×10^4. This method is reproducible in human induced pluripotent stem cells and is applied to model MNdegenerative diseases and in proof-of-principle drug screening assays.

[#]Corresponding author: Zhong-wei Du, PhD, Waisman Center, Rm622, University of Wisconsin, 1500 Highland Avenue, Madison, WI 53705, Phone (608)262-9441, zhongweidu@wisc.edu. Su-Chun Zhang, MD, PhD, Waisman Center, Rm 651, University of Wisconsin, 1500 Highland Avenue, Madison, WI 53705, Phone: (608) 265-2543, Fax: (608) 890-3479, zhang@waisman.wisc.edu.
[*]These authors contribute equally

Contributions

Z. D., H. C. and H. L. designed and performed experiments, analyzed data and prepared figures. J. L. established ALS and SMA hiPSC lines. K. Q., C. H., X. Z. and F. F. provide crucial data and reagents. Z. D. and S. Z. conceived the original idea, designed research, and wrote the manuscript.

Competing financial interests

The authors declare no competing financial interests.

INTRODUCTION

Human pluripotent stem cells (PSCs), including embryonic stem cells (ESCs) and induced pluripotent stem cells (iPSCs), offer a new model system to explore early human development and dissect disease processes, as well as an opportunity to devise therapeutics [1–3]. A critical requirement for achieving these potentials is directed differentiation of hPSCs to target cell types. Substantial progress has been made in guiding hPSCs to major cell lineages, including blood, cardiac, and neural cells [4–6]. Nevertheless, generation of highly-pure cellular populations in large quantities, which are often necessary for biochemical analysis, disease modeling, and clinical application, has not been readily achieved. In particular, it is often desired to obtain functionally specialized subtypes of cells from hPSCs, but these populations represent only a tiny fraction of the cells in a normal tissue/organ of our body. Such a need poses critical challenges to the stem cell field.

Spinal motor neurons (MNs) are a highly specialized type of neurons that reside in the ventral horns and project axons to muscles to control their movement. Degeneration of MNs is implicated in a number of devastating diseases, including spinal muscular atrophy (SMA), amyotrophic lateral sclerosis (ALS), Charcot-Marie-Tooth and poliomyelitis disease. The above disease iPSCs have been generated from patients and attempts have been made to identify disease-related phenotypes and to dissect out the underlying mechanisms before embarking on drug discovery [7–10]. However, these efforts are hindered by our inability to produce pure or highly enriched MNs with consistent quality. A number of protocols have been developed, including neural progenitor induction followed by neural patterning by retinoic acid (RA) and sonic hedgehog (SHH) [11, 12], neural progenitor induction followed by genetic manipulations using adenovirus-mediated gene delivery [13], and differentiation of MNs with above methods followed by sorting with GFP labeling under *MNX1* (also known as *HB9*) promoter [14]. These differentiation protocols are tedious, time consuming (1 to 2 months), and are of low efficiencies (30–70%) unless by sorting (90%). Furthermore, PSC-derived neurons in vitro, including MNs, are often immature, making it difficult to reveal disease phenotypes that are manifested in functionally mature cells. Hence, there is a critical need to develop new methods that enable generation of highly-pure and functionally mature MNs with consistent quality and in a short time.

By using a combination of small molecules in a chemical defined neural medium, we have guided hPSCs to a near-pure population of *OLIG2*$^+$ motor neuron progenitors (MNPs) in 12 days, and a highly enriched population of functionally mature MNs (>90%) in another 16 days by the use of a Notch inhibitor. Furthermore, our approach enables expanding a single MNP to 1×10^4 MNPs, producing a large quantity (5×10^5) of consistent MNs from a single stem cell. MNs generated by this method display molecular phenotypes of SMA and ALS, and can be readily adapted to screening platforms, as illustrated by our luciferase-based axonal length assay using ALS patient MNs.

RESULTS

Generation of highly-pure MNPs by a small-molecule cocktail

Specification of MNPs follows serial and overlapping developmental steps: neural induction as well as caudalization and ventralization of neuroepithelial progenitors (NEPs) [11, 15]. In the presence of small molecules, SB431542 (inhibitor of activin-nodal signaling, 2μM) and DMH1 (inhibitor of BMP signaling, 2μM) [16, 17], hESCs (line H9) were induced to NEPs, with 77±9% of the total differentiated cells being *SOX1*$^+$ (Fig. 1A, B). Activation of WNT by a small molecular agonist CHIR99021 has been shown to promote neural induction and potentially also neuroepithelial proliferation [18, 19]. Under the treatment of 3μM CHIR together with 2μM SB+2μM DMH for 6 days, nearly all the differentiated cells were *SOX1*$^+$ NEPs (>98%) (Fig. 1A, B). CHIR not only augmented the efficiency of neural induction, but also increased the yield of *SOX1*$^+$ NEPs by 2.8 fold (Fig. 1B). Wnt activation (by CHIR) often induces a caudal fate of neural progenitors [20]. Indeed, CHIR-induced NEPs showed a caudal identity with *HOXA3* expression. In contrast, NEPs induced by SB+DMH1 (without CHIR) exhibited a rostral identity with *OTX2* expression (Fig. 1B). Therefore, treatment of CHIR+SB+DMH combines the steps of induction and caudalization of NEPs, representing a chemically-defined, single-step method for obtaining homogenous caudal NEPs from hPSCs.

The next step is to specify *OLIG2*$^+$ MNPs by mimicking the ventralization of NEPs in vivo. By exposing the CHIR+SB+DMH-induced caudal-like NEPs to RA (0.1μM) and Pur (Purmorphamine, SHH signalling agonist, 1μM) for 6 days, which was identified in our previous study [21], we obtained 81±9% *OLIG2*-expressing neural progenitors (Fig. 1C). However, about 40% *OLIG2*$^+$ cells co-expressed with *NKX2.2*, another ventral spinal cord marker (Fig. 1C). During neural development, *OLIG2* and *NKX2.2* are initially induced in a common pool of progenitors that ultimately segregate into unique territories giving rise to distinct *OLIG2*$^+$ MNPs and *NKX2.2*$^+$ interneuron progenitors [22]. WNT signalling plays a critical role in this segregation [23]. We thus added WNT agonist CHIR in combination with RA and Pur. Under the treatment of CHIR+RA+Pur for 6 days, *NKX2.2* expression was completely repressed in the culture, but *OLIG2*-expressing population was also decreased to 62±5% (Fig. 1C). We reasoned that WNT signalling may elevate the threshold of SHH signalling necessary to induce *OLIG2* expression. However, at the increased concentration, SHH agonist Pur became toxic to the NEPs. We thus took an alternative approach to decrease the threshold of SHH signalling by repressing the dorsalizing molecule of the spinal cord, BMP signalling. Addition of dual SMAD inhibitors SB and DMH in combination with CHIR+RA+Pur significantly increased *OLIG2*$^+$/*NKX2.2*$^-$ cell population (Fig. 1C). By serial titration of Pur and CHIR in combination with RA, SB and DMH (Supplementary Fig. 1), we found that treatment with 1μM CHIR, 2μM SB, 2μM DMH, 0.1μM RA and 0.5μM Pur for 6 days resulted in a robust population of *OLIG2*$^+$ MNPs (95±3%), among which few (<0.5%) *OLIG2/NKX2.2* double positive cells were found (Fig. 1C).

Our protocol for *OLIG2*+ MNP specification is highly reproducible in multiple different hPSC lines, including normal iPSC line IMR90, ALS iPSC lines SOD1-D90A and SOD1-

A4V, and SMA iPSC lines SMA13 and SMA232 (Fig. 1D). Under the treatment of CHIR +SB+DMH1 for 6 days and CHIR+SB+DMH1+RA+Pur for another 6 days, all the hPSC lines generated more than 90% *OLIG2*$^+$ MNPs. Thus, coordinated specification and patterning of neuroepithelia by small molecules lead to robust generation of pure population of region-specific MNPs.

MNPs can be expanded to large numbers

Developmentally, *OLIG2*$^+$ MNPs are present transiently and they transition to other neuronal (interneuron) and glial (oligodendrocyte) lineages after generation of MNs. For cellular and biochemical analysis, it is crucial to expand the MNPs without losing their ability to produce MNs, which has not been achieved. Since the CHIR+SB+DMH1+RA +Pur condition is highly efficient in specifying and generating MNPs, we asked if the condition could expand the *OLIG2*$^+$ MNPs in a continuously dividing state. We first examined whether RA and Pur are required for maintaining *OLIG2* expression. The MNPs were passaged weekly under the CHIR+SB+DMH1 condition with or without Pur or RA +Pur. After two passages, *OLIG2*$^+$ MNPs were decreased to 35±5% in the control group (without Pur and RA), to 62±5% in Pur group, and a large population of *NKX2.2*$^+$ cells appeared in these two groups. In the RA+Pur group, OLIG2+ MNPs were maintained at 91±3% with rare *NKX2.2*$^+$ cells (Fig. 2A). Therefore, RA and Pur are required for maintaining the identity of MNPs.

We then examined whether CHIR, SB and DMH are required for maintaining cell proliferation. The MNPs were passaged under the RA+Pur condition and divided into three groups: SB+DMH treatment group, CHIR treatment group, and CHIR+SB+DMH treatment group. After two passages, the cell population expressing Ki-67, a cell proliferation marker, was at less than 8%, 81±6%, and 92±4% in the SB+DMH group, the CHIR group, and the CHIR+SB+DMH group, respectively (Fig. 2B). Therefore, CHIR+SB+DMH are required for maintaining the proliferation of MNPs at the maximum level.

When the MNPs were expanded in the same media (CHIR+SB+DMH+RA+Pur) for longer than two passages, the *OLIG2*-expressing MNP population decreased with a concomitant appearance of *MNX1* expressing MNs, suggesting that some MNPs have exited cell cycle and differentiated to neurons. We reasoned that this is likely due to the neurogenic effect of RA. It was known that valproate acid (VPA), a histone deacetylase inhibitor, can repress neurogenesis by indirectly activating Notch signalling [24]. We thus added VPA to the culture system. Under this culture condition, the MNPs were expanded for at least 5 passages yet maintained *OLIG2* expression at 82±9% (Fig. 2D). Further culturing under this condition resulted in gradual decrease of *OLIG2*$^+$ cell population and increase of *NKX2.2*$^+$ cell population, suggesting a need of alternative strategy for an even longer term expansion. Nevertheless, continual expansion of MNPs for 5 passages allows amplification of a single MNP to 1×10^4 MNPs, translating to the generation of $>5\times10^5$ MNPs from a single hPSC (Fig. 2E). Furthermore, these MNPs can be frozen and thawed in regular condition with over 90% recovery.

MNPs differentiate into an enriched population of functional MNs

To determine the differentiation of expanded MNPs, we withdrew CHIR+SB+DMH, increased RA concentration (0.5μM), and reduced Pur (0.1μM). After 6 days, nearly all the MNPs differentiated into MNs, as evidenced by expression of *MNX1* (90±9%) or *ISL1* (95±3%) (Fig. 3A, B). Further culture on Matrigel or astrocyte feeders for two weeks resulted in generation of more mature MNs that expressed *CHAT*, although the *CHAT*$^+$ MN population (47±9%) was substantially lower than the *MNX1*$^+$ MNPs. We reasoned that the lower population of *CHAT*$^+$ mature MNs may be due to proliferation of the small number of neural precursors and their subsequent differentiation to other neuronal types via lateral inhibition of NOTCH signaling [25]. To overcome this inefficiency of MN maturation, we applied Compound E (Cpd E), a NOTCH signaling inhibitor in the MN culture. CpdE treatment for 10 days resulted in a near homogenous MAP2$^+$ mature neuronal cultures without any proliferating cells (Ki67$^+$), and about 91±6% of MAP2$^+$ neurons expressed *CHAT* (Fig. 3A, B). These CHAT+MNs were electrophysiologically active, as defined by their ability to elicit action potentials in response to depolarizing current injection in current-clamp recordings (Supplementary Fig. 2). Therefore, CpdE not only increases the mature MN population but also substantially shortens the maturation process.

To determine whether the CpdE-accelerated MNs are functional, we co-cultured the MNs with differentiated myotubes from mouse C2C12 cells. After 10 days of co-culture, we observed aggregated BTX$^+$ acetylcholine receptors on myotubes and their overlapping with *CHAT*$^+$ neurites (Fig. 3C), suggesting formation of neuromuscular junctions. To study the ability of motor neurons to project axons toward the muscle targets, CpdE treated MNs were transplanted in ovo into the lesion neural tube of chicken embryos at HH stage15–16. Transplanted embryos showed successful engraftment of human MNs (as marked by GFP expression) into the ventral horn (Fig. 3D). Importantly, we observed GFP labelled human MN axons (*CHAT*$^+$) projected ventrally through the ventral roots and along the peripheral nerves of the host (Fig. 3D′). These data indicate that mature MNs generated by CpdE treatment exhibit proper functions.

Use of enriched MNs for disease modelling and screening

Most neurodegenerative diseases, like SMA and ALS, preferentially affect one type of neurons such as MNs. Genetically linked disorders, including SMA and ALS, may lead to changes in gene dosage at less than 50%. Hence, it will be technically difficult to discern changes in gene expression if the population of disease target cells is not highly enriched. To determine the utility of the MNs generated with the above method, we measured the expression of genes that are known to be altered in SMA and ALS. In this analysis, we generated spinal non-MNs from the same iPSCs as a control by replacing Pur with Cyclopamine (Cyc) to block SHH signaling (Supplementary Fig. 3A). Under RA and Cyc treatment for 6 days, the induced spinal neural precursors were void of *OLIG2* expression, and the differentiated neurons were void of *MNX1* and *CHAT* expression, but with GABA expression (Supplementary Fig. 3B, C). Using these highly enriched MNs and GABA neurons, we found that the mRNA of survival motor neuron (*SMN*) was decreased in both MNs and GABA neurons that were derived from SMA patients as compared to those from non-SMA iPSCs (Fig. 4A). This is consistent with the fact that *SMN* mutations affect all cell

types. Interestingly, we found that MNs exhibited even lower (38±4%) *SMN* than that in GABA neurons (60±6%) (Fig. 4A), again consistent with a previous report that MNs express markedly lower levels of full-length SMN transcripts from *SMN2* gene than do other cells in the spinal cord [26]. Similarly in ALS caused by mutations in superoxide dismutase (*SOD1*) gene, MNs display neurofilament (NF) aggregation that is attributed to the decreased level of light polypeptide neurofilament (*NEFL*) [9], we found a 45±4% reduction of *NEFL* mRNA in D90A MNs, but not GABA neurons, when compared to genetically corrected (D90D) MNs and GABA neurons (Fig. 4B). Together, these data indicate that the enriched MNs generated from patient iPSCs using our new method enable identification of disease related phenotypes.

Our ability to generate large quantity of consistent MNs offers an opportunity for building high-throughput screening platforms for MN diseases. In ALS, astrocytes enhance disease progression by promoting axonal degeneration and MN death [27–29]. Indeed, when ALS iPSC-derived MNs were grown on top of ALS (D90A SOD1) or genetically corrected (D90D *SOD1*) astrocytes (Supplementary Fig. 4) in a medium that lacks neurotrophic factors, MNs began to show neurite fragmentation with reduced neurite length on D90A but not D90D astrocytes at Day10 (Fig. 4C). To enable automated measurement of neurite length for high throughput screening, we established a reporter iPSC line (from D90A *SOD1*) with a luciferase reporter NanoLuc (Nluc) fused with SYNAPTOPHYSIN (SYP) (Fig. 4D), a synaptic vesicle glycoprotein, which targets the Nluc reporter to axonal membrane, not cytoplasm [30]. We first established the linear relationship between Nluc expression and MN numbers by measuring luciferase activity of cultures 10 days after plating different numbers of SYP-Nluc expressing MNs (1250, 2500, 5000, 10000 and 20000 cells) on astrocytes (Supplementary Fig. 5A). We then tested whether the Nluc reporter activity is correlated with the reduced axonal length. Same numbers of SYP-Nluc expressing MNs were plated on D90D and D90A astrocytes and the Nluc activity was detected at Day10. The Nluc activity on D90A astrocytes was significantly decreased to 70.5±2.7%, comparing to the D90D astrocyte group (Supplementary Fig. 5B). Next, we exposed the co-cultures to three compounds, Riluzole (Rilu) [31], the only approved drug for ALS, as well as Kenpaullone (Ken) and EphA inhibitor (EphAi) that are known to rescue axonal degeneration in ALS cell models [32, 33]. Riluzole had no effect on Nluc activity. Ken and EphAi increased the Nluc activity to 1.5 and 2.8 fold in both D90A and D90D groups (Fig. 4E), indicating that they increased axonal length. However, Ken and EphAi did not specifically rescue the axonal length of MNs induced by ALS astrocytes, as the ratio of Nluc activity on D90A astrocytes versus D90D astrocytes remained at 70% (Fig. 4E). These results provide a proof of principle for the use of our enriched, patient-derived MNs for drug screening and suggest its potential for identifying disease specific targets.

DISSCUSSION

We have developed a strategy for guiding hPSCs to a near-pure population of *OLIG2*$^+$ MNPs in 12 days by coordinating signaling pathways using small molecules, and subsequently a highly enriched population of functionally mature MNs (>90%) in another 16 days by the use of a Notch inhibitor. Furthermore, we have devised a method to expand a single MNP to 1×10^4 MNPs, enabling production of a large quantity (5×10^5) of consistent

MNs from a single stem cell. Our approach enables presentation of disease phenotypes and building of screening platforms, as illustrated by our luciferase-based axonal length assay using ALS patient MNs.

Compared to previous methods, our method has two critical improvements. The first is the application of WNT agonist during MNP differentiation. WNT signaling is a more efficient pathway to caudalize neural progenitors [20]. Thus, the combination of WNT activator with dual SMAD inhibitors induced homogenous caudal NEPs from hPSCs. Most importantly, WNT signaling plays a critical role in MNP specification. All previous methods used RA and SHH to induce *OLIG2*$^+$ MNPs without examining other ventral spinal markers, especially co-expression of *NKX2.2*. We showed here that RA and SHH condition generated mixed ventral progenitors with a large population of cells that co-express *OLIG2* and *NKX2.2*. During spinal cord development, *OLIG2* and *NKX2.2* are initially induced in a common pool of progenitors that ultimately segregate into unique territories, giving rise to distinct *OLIG2*$^+$ MNPs (pMN domain) and *NKX2.2*$^+$ interneuron progenitors (p3 domain) [22]. Without segregation, *NKX2.2* could interfere with the differentiation of *OLIG2*$^+$ progenitors to *MNX1*$^+$ MNs, which is one of the reasons why some previous methods induced a high percentage of *OLIG2*$^+$ progenitors, but ended with a small population of *MNX1*$^+$ MNs. WNT signaling was reported to selectively oppose SHH-mediated induction of NKX2.2, but have little effect on OLIG2, and thereby establish their distinct expression domains in cooperation with graded SHH signaling [23]. As WNT elevates the strength of SHH signaling to induce *OLIG2* expression, the two inhibitors of dorsalizing BMP signaling were also included. Therefore, our method of combining with small molecules regulating WNT, SHH, RA and BMP signalings closely mimics the cooperation of these signalings in the spinal cord development in vivo to specify the region-specific *OLIG2*$^+$ MNPs. Recently Maury et al. also applied WNT agonist CHIR in the generation of MNs from hPSCs [34]. However, the treatment condition under which CHIR was applied is different, and the NKX2.2-expressing cell population was not examined. It will be interesting to compare two approaches in specifying MNPs.

The second improvement is the application of a NOTCH inhibitor during MN maturation. Lateral inhibition mediated by NOTCH signaling is an intrinsic mechanism to guide orderly transition of mitotically active precursors into different types of post-mitotic neurons and glia at different stages [25]. The treatment with NOTCH inhibitor CpdE in our method synchronizes the differentiation of *OLIG2*$^+$ MNPs to generate homogenous mature MNs without mixing with any other neural cells. With these two improvements, our method robustly generates almost homogenous mature MNs, which exhibit functional properties, including formation of neuromuscular junctions when co-cultured with skeletal muscle cells and projection of axons toward muscles when grafted into the developing chick spinal cord. More significantly, the MNs derived from disease iPSCs by our method exhibit the MN-specific molecular phenotypes, including downregulation of full-length SMN in SMA and downregulation of NEFL level in ALS, which would be nearly impossible to detect with previous methods that only generate a small population of MN in the mixed culture.

A large quantity of consistent target cells, such as mature MNs, is necessary for high-throughput screening. In general, lineage committed progenitors can be expanded, but

quickly lose their differentiation potency. For example, *OLIG2*$^+$ MNPs can be expanded with FGF and/or EGF, but quickly lose the potency of MN differentiation in two passages. Several recent reports described the expansion of neural progenitors with small molecules of WNT and/or SHH signalings [18, 35]. However, as shown in this study (Fig. 2A), their ability to maintain MN potential is still significantly diminished during cell passages compared to our method. Our method can expand MNPs for at least 5 passages to amplify a single MNP to 1×10^4 MNPs, or generate 5×10^5 MNs from single hPSC. This provides a sufficient cell source for high-throughput drug screening, as shown in our screening platform for MN axonal degeneration. In summary, our new method enables generation of large quantities of MNs with consistency and high purity, providing a basis for modeling MN diseases in vitro and for drug discovery.

METHODS

Human pluripotent stem cells (PSCs)

The human PSC lines used in this study are listed in Supplementary Table 1. Fibroblasts from a 50-y-old female ALS patient carrying the D90A SOD1 mutation (ND29149, Coriell Institute, coriell.org), a 3-y-old male SMA patient (GM03813, Coriell Institute) and a 7-m-old SMA patient (GM00232, Coriell Institute) were reprogrammed using the non-integrating Sendai virus as described (Ban et al., 2011) to established iPSC lines ALS-D90A, SMA13 and SMA232. D90D iPSC line was established by correcting the D90A *SOD1* mutation in ALS-D90A lines by TALEN technology (Chen et al., 2014). A4V *SOD1* mutant ALS iPSC line, established with retrovirus, was obtained from Coriell (ND35671). Human ESC line H9 (WA09 line, NIH registry 0046) and normal iPSC line IMR90-4 were obtained from WiCell. All the PSCs were cultured on irradiated mouse embryonic fibroblasts (MEFs) as described in the standard protocol http://www.wicell.org.

MNP specification and MN differentiation

To generate MNPs, hPSCs were dissociated with Dispase (1 mg/ml) and split 1:6 on irradiated MEFs or Matrigel coated plates. On the following day, the PSC medium was replaced with a chemically defined neural medium, including DMEM/F12, Neurobasal medium at 1:1, 0.5×N2, 0.5×B27, 0.1mM ascorbic acid (Santa Cruz), 1×Glutamax and 1×penicillin/streptomycin (All others from Invitrogen). CHIR99021 (3uM, Torcris), 2μM DMH-1 (Torcris) and 2μM SB431542 (Stemgent) were added in the medium. The culture medium was changed every other day. Human PSCs maintained under this condition for 6 days were induced into NEP cells. The NEP cells were then dissociated with Dispase (1 mg/ml) and split at 1:6 with the same medium described above. RA (0.1μM, Stemgent) and 0.5μM Purmorphamine (Stemgent) were added in combination with 1μM CHIR99021, 2μM DMH-1, and 2μM SB431542. The medium was changed every other day. NEP cells maintained under this condition for 6 days differentiated into OLIG2+ MNPs. The *OLIG2*$^+$ MNPs were expanded with the same medium containing 3μM CHIR99021, 2μM DMH-1, 2μM SB431542, 0.1μM RA, 0.5μM Purmorphamine and 0.5 mM VPA (Stemgent), and split 1:6 once a week with Dispase (1 mg/ml). *OLIG2*$^+$ MNPs were frozen with the regular frozen medium (DMEM/F12, 10% fetal bovine serum and 10% DMSO) in liquid nitrogen, and cultured again in expansion medium after thawing.

To induce MN differentiation, *OLIG2*$^+$ MNPs were dissociated with Dispase (1 mg/ml) and cultured in suspension in the above neural medium with 0.5μM RA and 0.1μM Purmorphamine. The medium was changed every other day. *OLIG2*$^+$ MNPs under this condition for 6 days differentiated into *MNX1*$^+$ MNs. The *MNX1*$^+$ MNs were then dissociated with Accumax (eBioscience) into single cells and plated on Matrigel coated plates or on astrocytes. The *MNX1*$^+$ MNs were cultured with 0.5μM RA, 0.1μM Purmorphamine and 0.1μM Compound E (Calbiochem) for 10 days to mature into CHAT$^+$ MNs. Insulin-like growth factor 1(IGF-1), brain-derived neurotrophic factor (BDNF), and ciliary neurotrophic factor (CNTF) (all from R&D, 10 ng/ml each) were added if MNs were plated at low density. For identifying MN disease phenotypes, SMA and ALS MNs were cultured without these neurotrophic factors.

Functional analysis of mature MNs

Whole-cell patch-clamp recordings were performed on iPSC-derived CHAT$^+$ neurons at Day28 after iPSC differentiation. Briefly, neurons were held at −70mV to record Na+/K+ channel activities, and at 0mV to record spontaneous release. For recording action potentials, cells were held at 0 pA with the current-clamp model and the steps of currents from +0 pA were injected into cells by the holding electrode. The bath solution consisted of 127 mM NaCl, 1.2 mM KH2PO4, 1.9 mM KCl, 26 mM NaHCO3, 2.2 mM CaCl2, 1.4 mM MgSO4, 10 mMglucose, 290 mM mOsm and 95% O2/5% CO2. Recording pipettes were filled with an intracellular solution containing 20 mM KCl, 121 mM K+-gluconate, 10 mM Na+-HEPES, 10 mM BAPTA, 4 mM Mg2+-ATP pH 7.2 and 290 mOsm. An Olympus BX51WI microscope was used to visualize neurons. A MultiClamp 700B amplifer (Axon instruments, Molecular Devices, Sunnyvale, CA, USA) was used to investigate the voltage clamp and current clamp recordings. Signals were filtered at 4 kHZ and sampled at 100 kHz using a Digidata 1322A analog-digital converter (Axon instruments). Data were analyzed with pClamp 9.0 (Axon instruments). Capacitance and series resistance were compensated by 50–80% using an amplifier circuitry.

To examine neuromuscular junction formation, C2C12 cells were seeded on Matrigel coated plate in DMEM with 10% FBS, and then were induced to form myotube by switching to DMEM containing 2% FBS. Day18 *MNX1*$^+$ MNs derived from hPSCs were plated onto myotubes and cultured in maturation condition for 7 days, after which the neuromuscular synapses were visualized using CHAT and BTX staining.

To perform transplantations, Day-18 *MNX1*$^+$ MN spheres were triturated with a 1-ml pipette tip 5–7 times and treated with CpdE for 24hrs. Transplantation was performed as previously described[15]. Briefly, after a small suction lesion at the prospective intraspinal site was created in a chick embryo at stage 15–18 at somites 15–20, MN spheres were loaded into a handheld micro-injector and placed into the lesion. After 6 days, the chicks were sacrificed, fixed with 4% PFA for 2 h at 4°C, and neurite outgrowth was accessed by cutting 30μm sections of the spinal cord near the injected site.

qPCR analysis

Total RNAs were isolated with RNeasy Plus Mini Kit (Qiagen) according to the manufacturer's instructions. For qPCR, cDNA was synthesized from 1ug total RNAs using iScript™ reverse transcription supermix (Biorad). qPCR was performed using iTaq™ Universal SYBR® Green Supermix (Biorad). GAPDH gene was used as internal control to equalize cDNA. The following primers were used in this study:

Full length SMN, forward-CACCACCTCCCATATGTCCAGATT,

reverse-GAATGTGAGCACCTTCCTTCTTT;

Total SMN, forward- ATGAGCTGTGAGAAGGGTGTTG,

reverse-TTGCCACATACGCCTCACATAC;

NEFL, forward-TTTCACTCTTTGTGGTCCTCA,

reverse-AGACCCTGGAAATCGAAGC;

GAPDH, forward-CTCTCTGCTCCTCCTGTTCGAC,

reverse-TGAGCGATGTGGCTCGGCT.

Immunostaining and microscopy

Immunohistochemical staining was performed according to Zhang et al (2001). The following primary antibodies were used: SOX1 (gIgG 1:1000, R&D), OTX2 (mIgG, 1:2000, DSHB), HOXA3 (mIgG 1:1000, R&D), OLIG2 (rIgG 1:500, Chemicon), NKX2.2 (mIgG 1:100, DSHB), Ki67 (rIgG 1:200, Chemicon), MNX1 (mIgG 1:50, DSHB), ISL1 (mIgG 1:1000, DSHB), TUJ1 (rIgG 1:5000, Covance), CHAT (gIgG 1:300, Chemicon), MAP2 (mIgG 1:1000, Chemicon), GABA (mIgG 1:1000, Chemicon), FoxP1 (rIgG, 1:1000, Chemicon).

MN-astrocyte co-culture and Luciferase assay

The luciferase reporter NanoLuc (Nluc) was obtained from Promega. The SYP-Nluc reporter iPSC line was established by inserting SYP-Nluc fusion reporter in the AAVS1 site by the TALEN technology (Qian et. al, 2014). 6-month Astrocytes were differentiated from the isogenic iPSC lines D90D and D90A by the protocol established in our lab (Krencik et. al, 2011). The astrocytes were plated at 1×10^4 cells/well in white 96-well plates (Greiner Bio-one) and cultured in the astrocyte medium (DMEM, 10% FBS) for 7 days. The D90A MNX1+ MNs derived from SYP-Nluc reporter iPSC line were the plated at 1×10^4 cells/well on astrocytes and cultured in a nutrition deficient medium (DMEM/F12, Neurobasal medium at 1:1, 1×N2, 0.5μM RA and 0.1μM Compound E). For testing the compounds, Riluzole (50μM, Torcris), Kenpaullone (5μM, Tocris) and EphA inhibitor (50μM, Calbiochem) were added in the medium. After coculturing for 10 days, the Nluc activity was detected by Nano-Glo® Luciferase Assay (Promega) according to the manufacturer's instructions.

Statistical analyses

No statistical methods were used to predetermine sample sizes, but the samples sizes we used were consistent with those generally employed in the field. Comparisons between two groups were analyzed by unpaired t-test with Welch's correction. Multiple comparisons were analyzed by one-way analysis of variance followed by Tukey's multiple comparisons test. $P<0.05$ was considered to be statistically significant. Statistical processing was performed using Microsoft Excel and GraphPad Prism Software.

Supplementary Material

Refer to Web version on PubMed Central for supplementary material.

Acknowledgments

This study was supported by NIH-NINDS grants (NS045926 and NS064578 for S. Zhang, NS074189 and NS085689 for Z. Du) and in part by a core grant to the Waisman Center from the National Institute of Child Health and Human Development (P30 HD03352).

References

1. Grskovic M, Javaherian A, Strulovici B, Daley GQ. Induced pluripotent stem cells--opportunities for disease modelling and drug discovery. Nat Rev Drug Discov. 2011; 10:915–929. [PubMed: 22076509]
2. Han SS, Williams LA, Eggan KC. Constructing and deconstructing stem cell models of neurological disease. Neuron. 2011; 70:626–644. [PubMed: 21609821]
3. Goldman SA, Nedergaard M, Windrem MS. Glial progenitor cell-based treatment and modeling of neurological disease. Science. 2012; 338:491–495. [PubMed: 23112326]
4. Ma F, et al. Generation of functional erythrocytes from human embryonic stem cell-derived definitive hematopoiesis. Proc Natl Acad Sci U S A. 2008; 105:13087–13092. [PubMed: 18755895]
5. Kattman SJ, et al. Stage-specific optimization of activin/nodal and BMP signaling promotes cardiac differentiation of mouse and human pluripotent stem cell lines. Cell Stem Cell. 2011; 8:228–240. [PubMed: 21295278]
6. Liu H, Zhang SC. Specification of neuronal and glial subtypes from human pluripotent stem cells. Cell Mol Life Sci. 2011; 68:3995–4008. [PubMed: 21786144]
7. Ebert AD, et al. Induced pluripotent stem cells from a spinal muscular atrophy patient. Nature. 2009; 457:277–280. [PubMed: 19098894]
8. Egawa N, et al. Drug screening for ALS using patient-specific induced pluripotent stem cells. Sci Transl Med. 2012; 4:145ra104.
9. Chen H, et al. Modeling ALS with iPSCs reveals that mutant SOD1 misregulates neurofilament balance in motor neurons. Cell Stem Cell. 2014; 14:796–809. [PubMed: 24704493]
10. Kiskinis E, et al. Pathways disrupted in human ALS motor neurons identified through genetic correction of mutant SOD1. Cell Stem Cell. 2014; 14:781–795. [PubMed: 24704492]
11. Li XJ, et al. Specification of motoneurons from human embryonic stem cells. Nat Biotechnol. 2005; 23:215–221. [PubMed: 15685164]
12. Qu Q, et al. High-efficiency motor neuron differentiation from human pluripotent stem cells and the function of Islet-1. Nat Commun. 2014; 5:3449. [PubMed: 24622388]
13. Hester ME, et al. Rapid and efficient generation of functional motor neurons from human pluripotent stem cells using gene delivered transcription factor codes. Mol Ther. 2011; 19:1905–1912. [PubMed: 21772256]
14. Amoroso MW, et al. Accelerated high-yield generation of limb-innervating motor neurons from human stem cells. J Neurosci. 2013; 33:574–586. [PubMed: 23303937]

15. Wichterle H, Lieberam I, Porter JA, Jessell TM. Directed differentiation of embryonic stem cells into motor neurons. Cell. 2002; 110:385–397. [PubMed: 12176325]
16. Chambers SM, et al. Highly efficient neural conversion of human ES and iPS cells by dual inhibition of SMAD signaling. Nat Biotechnol. 2009; 27:275–280. [PubMed: 19252484]
17. Neely MD, et al. DMH1, a highly selective small molecule BMP inhibitor promotes neurogenesis of hiPSCs: comparison of PAX6 and SOX1 expression during neural induction. ACS Chem Neurosci. 2012; 3:482–491. [PubMed: 22860217]
18. Li W, et al. Rapid induction and long-term self-renewal of primitive neural precursors from human embryonic stem cells by small molecule inhibitors. Proc Natl Acad Sci U S A. 2011; 108:8299–8304. [PubMed: 21525408]
19. Lu J, et al. Generation of integration-free and region-specific neural progenitors from primate fibroblasts. Cell Rep. 2013; 3:1580–1591. [PubMed: 23643533]
20. Xi J, et al. Specification of midbrain dopamine neurons from primate pluripotent stem cells. Stem Cells. 2012; 30:1655–1663. [PubMed: 22696177]
21. Li XJ, et al. Directed differentiation of ventral spinal progenitors and motor neurons from human embryonic stem cells by small molecules. Stem Cells. 2008; 26:886–893. [PubMed: 18238853]
22. Lee SK, Pfaff SL. Transcriptional networks regulating neuronal identity in the developing spinal cord. Nat Neurosci. 2001; 4 (Suppl):1183–1191. [PubMed: 11687828]
23. Wang H, Lei Q, Oosterveen T, Ericson J, Matise MP. Tcf/Lef repressors differentially regulate Shh-Gli target gene activation thresholds to generate progenitor patterning in the developing CNS. Development. 2011; 138:3711–3721. [PubMed: 21775418]
24. Stockhausen MT, Sjölund J, Manetopoulos C, Axelson H. Effects of the histone deacetylase inhibitor valproic acid on Notch signalling in human neuroblastoma cells. Br J Cancer. 2005; 92:751–759. [PubMed: 15685243]
25. Lewis J. Notch signalling and the control of cell fate choices in vertebrates. Semin Cell Dev Biol. 1998; 9:583–589. [PubMed: 9892564]
26. Ruggiu M, et al. A role for SMN exon 7 splicing in the selective vulnerability of motor neurons in spinal muscular atrophy. Mol Cell Biol. 2012; 32:126–138. [PubMed: 22037760]
27. Di Giorgio FP, Carrasco MA, Siao MC, Maniatis T, Eggan K. Non-cell autonomous effect of glia on motor neurons in an embryonic stem cell-based ALS model. Nat Neurosci. 2007; 10:608–614. [PubMed: 17435754]
28. Nagai M, et al. Astrocytes expressing ALS-linked mutated SOD1 release factors selectively toxic to motor neurons. Nat Neurosci. 2007; 10:615–622. [PubMed: 17435755]
29. Haidet-Phillips AM, et al. Astrocytes from familial and sporadic ALS patients are toxic to motor neurons. Nat Biotechnol. 2011; 29:824–828. [PubMed: 21832997]
30. Nakata T, Terada S, Hirokawa N. Visualization of the dynamics of synaptic vesicle and plasma membrane proteins in living axons. J Cell Biol. 1998; 140:659–674. [PubMed: 9456325]
31. Miller RG, Mitchell JD, Moore DH. Riluzole for amyotrophic lateral sclerosis (ALS)/motor neuron disease (MND). Cochrane Database Syst Rev. 2012; 3:CD001447. [PubMed: 22419278]
32. Yang YM, et al. A small molecule screen in stem-cell-derived motor neurons identifies a kinase inhibitor as a candidate therapeutic for ALS. Cell Stem Cell. 2013; 12:713–726. [PubMed: 23602540]
33. Van Hoecke A, et al. EPHA4 is a disease modifier of amyotrophic lateral sclerosis in animal models and in humans. Nat Med. 2012; 18:1418–1422. [PubMed: 22922411]
34. Maury Y, et al. Combinatorial analysis of developmental cues efficiently converts human pluripotent stem cells into multiple neuronal subtypes. Nat Biotechnol. 2015; 33:89–96. [PubMed: 25383599]
35. Reinhardt P, et al. Derivation and expansion using only small molecules of human neural progenitors for neurodegenerative disease modeling. PLoS One. 2013; 8:e59252. [PubMed: 23533608]

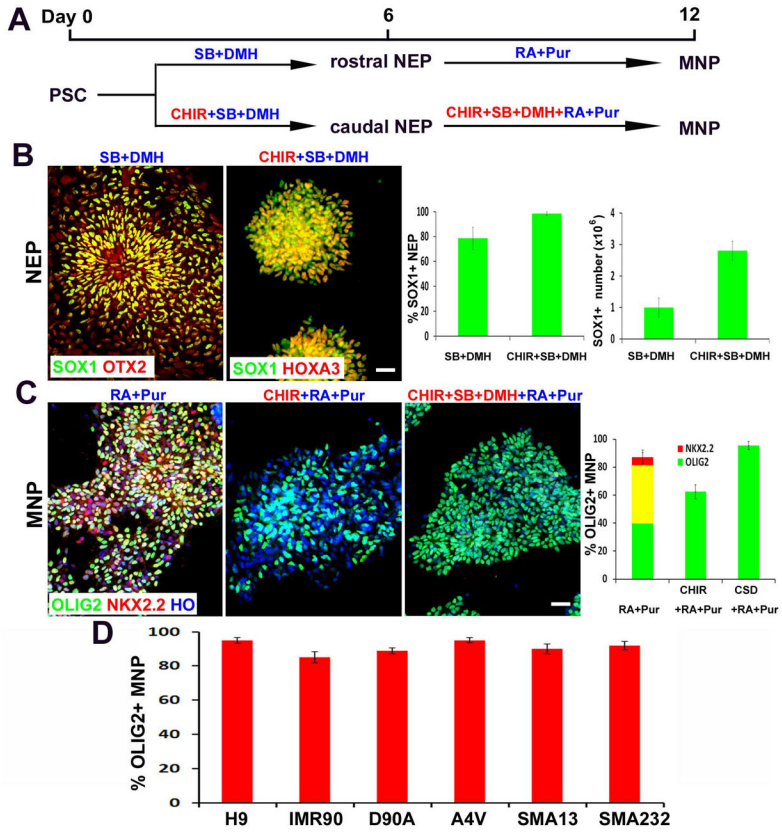

Figure 1. Generation of highly-pure population of MNPs from hPSCs

(A) Schematics showing the time course and small molecule cocktail for hPSC differentiation into MNPs. (B) Representative images of *SOX1*+ NEPs after 6 days of culture in CHIR+SB+DMH vs. SB+DMH condition. The regional identity (*OTX2*+ vs. *HOXA3*+) were stained. Scale bars: 50μm. Quantification of *SOX1*+ NEP percentage and number is shown on right (>500 cells from random fields were manually counted in each condition). The bar graph shows the mean±s.d. (n=3 in each condition). (C) Representative images of pure MNPs at Day12 under different conditions, which express *OLIG2* (green) but not *NKX2.2* (red). Scale bars: 50μm. Quantification of *OLIG2*+, *NKX2.2*+ and *OLIG2*+/*NKX2.2*+ cells is shown on right (>500 cells from random fields were manually counted in each condition). The bar graph shows the mean±s.d. (n=3 in each condition). (D) The efficiency of *OLIG2*$^{+}$ MNP differentiation from multiple hPSC lines (>500 cells from random fields were manually counted in each cell line). The bar graph shows the mean±s.d. (n=3 in each cell line).

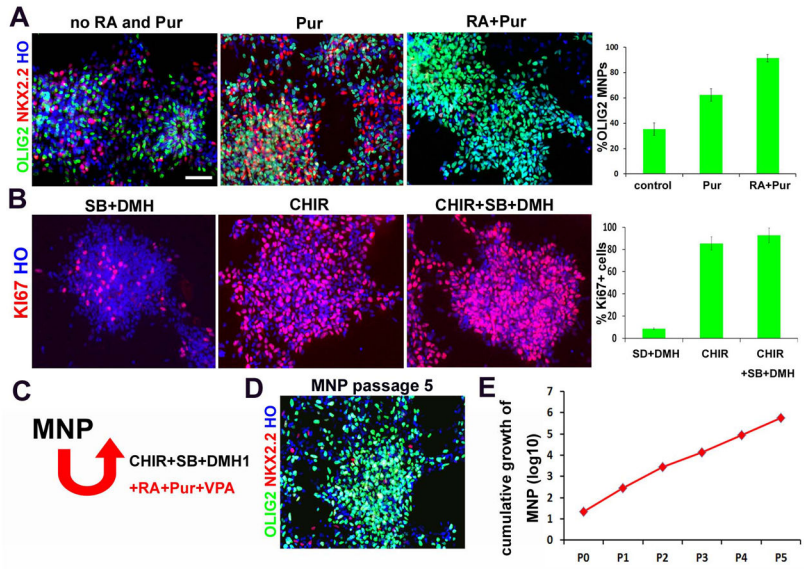

Figure 2. Expansion of *OLIG2*$^{+}$ MNPs

(A) Representative images of pure *OLIG2*+ (green)/*NKX2.2*$^{+}$ (red) MNPs maintained under different conditions. Scale bars: 50μm. Quantification of *OLIG2*+/*NKX2.2*− cells is shown on right (>500 cells from random fields were manually counted in each condition). The bar graph shows the mean±s.d. (n=3 in each condition). (B) Representative images of *Ki67*+ (red) proliferating progenitors maintained under different conditions. Scale bars: 50μm. Quantification of *Ki67*$^{+}$ cells is shown on right (>500 cells from random fields were manually counted in each condition). The bar graph shows the mean±s.d. (n=3 in each condition). (C) Schematics showing the expansion of MNPs with the combination of small molecules. (D) Representative images of MNPs expanded for at least 5 passages yet maintained the OLIG2 (green) expression. (E) Cumulative hPSC-derived MNP counts over five passages (passages denoted p1–p5). One 6-well of cells were manually counted in each passage, and total cell numbers were calculated by times passage ratio.

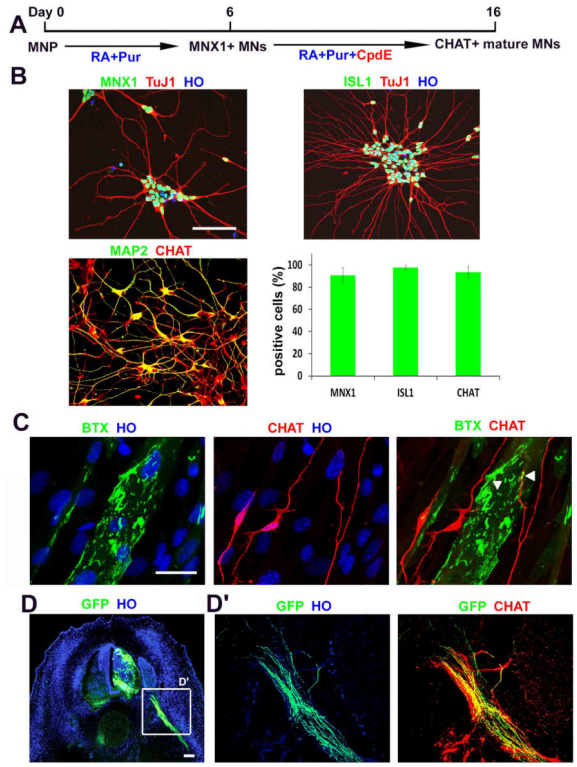

Figure 3. MNPs differentiate into enriched functional MNs

(A) Schematics showing the time course and small molecule cocktail for MNP differentiation into mature MNs. (>500 cells from random fields were manually counted in each condition). The bar graph shows the mean±s.d. (n=3 in group). (B) Representative images of MNs showing *MNX1*$^{+}$, *ISL1*$^{+}$ (green) and *CHAT*$^{+}$ (red) on. Scale bars: 50μm. Quantification of *MNX1*$^{+}$, *ISL1*$^{+}$ and *CHAT*$^{+}$ is shown (C) MNs, stained with CHAT antibody (red), formed neuromuscular junctions, labelled with bungarotoxin (BTX, green), when co-cultured with myotubes. Scale bars: 100μm. (D) Representative image of xenotransplantation of GFP labeled human MNs into a developing chicken embryo. Scale bars: 50μm. (D′) magnification of the field showing that human MN axons (GFP^{+}/*CHAT*$^{+}$) projected ventrally through the ventral roots.

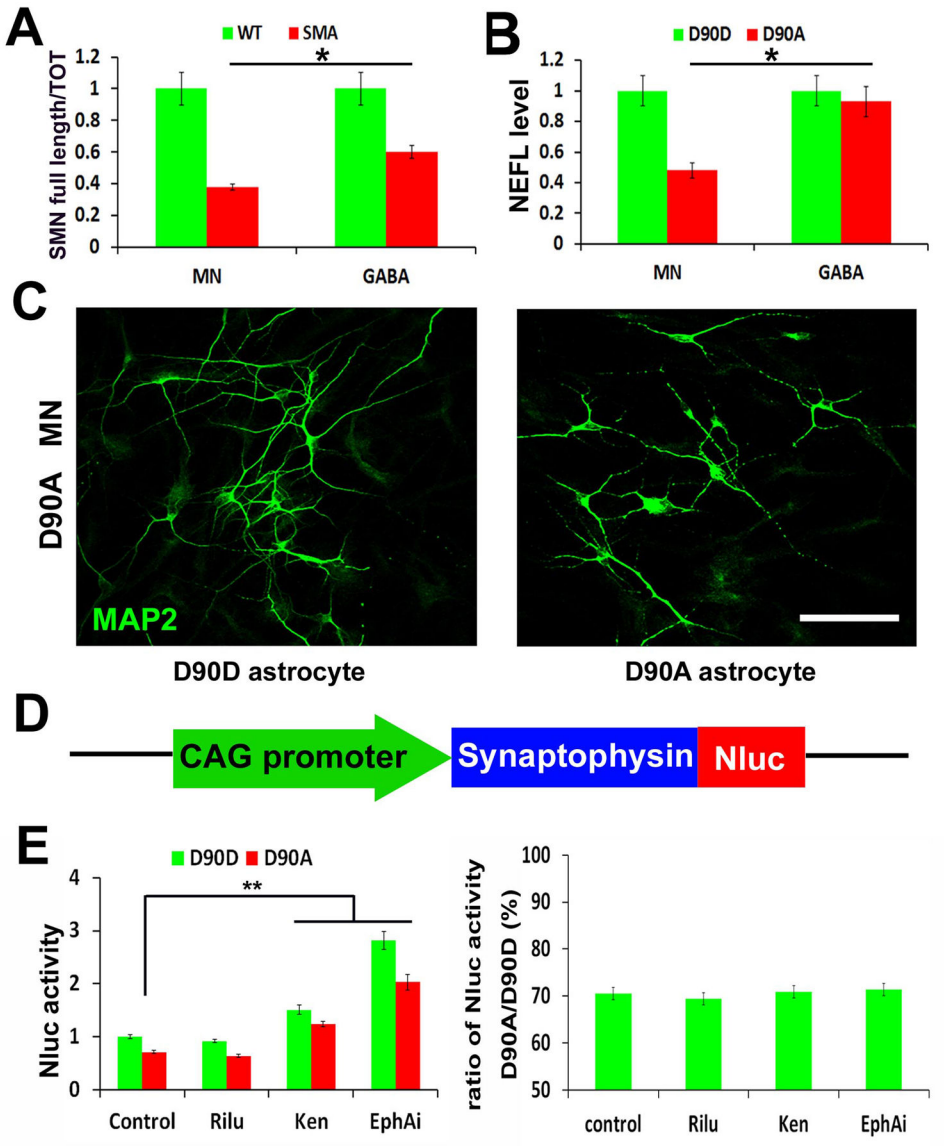

Figure 4. Enriched MNs for disease modelling and screening

(A) The qPCR quantification of the ratio of full length SMN vs. total SMN in wildtype (WT) and SMA disease MNs, GABA neurons. The bar graph shows the mean±s.e.m. (*p<0.05, t-test, n= 3 in each group). (B) The qPCR quantification of *NEFL* mRNA level in ALS (D90A) and corrected (D90D) MNs, GABA neurons. The bar graph shows the mean ±s.e.m. (*p<0.05, t-test, n= 3 in each group). (C) Representative image of ALS (D90A) MNs when culturing on ALS (D90A) astrocytes and corrected (D90D) astrocytes, which showed neurite fragmentation and reduced neurite length. Scale bars: 50μm. (D) Schematics of SYP-Nluc reporter. (E) Quantification of Nluc activity (left panel) and ratio (right panel) of SYP-Nluc reporter MNs on ALS (D90A) and corrected (D90D) astrocytes, when comparing between the control, Riluzole (Rilu), Kenpaullone (Ken) and EphA inhibitor

(EphAi) groups. The bar graph shows the mean±s.e.m. (** P<0.01, Tukey's test, n= 8 in each group).